RESEARCH ARTICLE | NOVEMBER 25 2024

A numerical study on unsteadiness of vertical flow around a horizontal heated square cylinder with variable thermal buoyancy

Shima Yazdani ; Erfan Salimipour ; Mikhail Sheremet ; Mohammad Ghalambaz

Physics of Fluids 36, 113626 (2024)
https://doi.org/10.1063/5.0235800

Physics of Fluids ARTICLE pubs.aip.org/aip/pof

A numerical study on unsteadiness of vertical flow around a horizontal heated square cylinder with variable thermal buoyancy

Cite as: Phys. Fluids **36**, 113626 (2024); doi: 10.1063/5.0235800
Submitted: 29 August 2024 · Accepted: 3 November 2024 ·
Published Online: 25 November 2024

Shima Yazdani,[1] Erfan Salimipour,[2,a)] Mikhail Sheremet,[1] and Mohammad Ghalambaz[1,3]

AFFILIATIONS

[1]Laboratory on Convective Heat and Mass Transfer, Tomsk State University, 634050 Tomsk, Russia
[2]Department of Mechanical Engineering, Faculty of Advanced Technologies, Quchan University of Technology, Quchan, Iran
[3]Department of Mathematics, Saveetha School of Engineering, SIMATS, Chennai, India

[a)]Author to whom correspondence should be addressed: esalimipour@qiet.ac.ir

ABSTRACT

Analyzing the unsteadiness of flow is crucial due to its significant influence on flow characteristics, and at times, it can even alter the flow pattern entirely. In this research, the effects of two distinct types of unsteadiness—thermal buoyancy and vortex shedding—were examined in the context of laminar flow around a square cylinder. Initially, the impact of each unsteady phenomenon on the flow was studied independently. Subsequently, the combined influence of both unsteady factors on the flow was assessed. The Navier–Stokes equations are solved using a finite-volume approach, which discretizes the computational domain into small control volumes. This technique integrated a pressure-based method with a symmetry-preserving technique, which minimizes numerical diffusion, making it well-suited for accurately capturing flow instabilities. An in-house solver was developed specifically for this purpose. The calculations were conducted for Richardson numbers (Ri) ranging from 0 to 0.35 and for three different Prandtl numbers (Pr) of 0.2, 0.7, and 2.5, all at a Reynolds number (Re) of 100. Vortex shedding, referred to as type 1 unsteadiness, occurs naturally at Re = 100. To induce type 2 unsteadiness, Richardson numbers were varied according to a sinusoidal equation. The findings revealed that the drag coefficient of the cylinder is significantly affected by the frequency of Richardson numbers' variation. As the variation frequency decreased, the difference in drag coefficients during the increasing and decreasing phases of Ri also diminished.

NOMENCLATURE

a	Cylinder's length
C_d	Drag coefficient
C_l	Lift coefficient
k	Reduced frequency
Pr	Prandtl number
Re	Reynolds number
Ri	Richardson number
St	Strouhal number
T_s	Surface temperature
T_∞	Free-stream temperature
V_∞	Free-stream velocity
Θ	Non-dimensional temperature

I. INTRODUCTION

For more than a century, the flow around cylinders has been extensively studied, particularly in the context of bluff body wake dynamics, laying the groundwork for much of the fundamental research in this field.[1–4] Typically, these investigations involve cylinders with circular or square cross sections, though studies have also explored cylinders with oval cross sections.[5–7] Fluid flows are generally categorized into steady and unsteady types. In steady flows, the flow characteristics remain constant over time, whereas in unsteady flows, these characteristics vary with time. Unsteadiness in flow can manifest in three distinct ways:

Type 1 (Unsteadiness in the flow's intrinsic nature): This type typically occurs in flows around blunt bodies due to vortex shedding.[8] For asymmetric bluff bodies or those at an angle of attack, vortex shedding results from uneven forces, inducing oscillations in both the flow field and aerodynamic coefficients. Even symmetric bodies like cylinders can experience vortex shedding at critical Reynolds numbers when disturbances in the flow grow, causing asymmetric flow patterns and unsteady wake dynamics. Vortex shedding can lead to flow-induced vibrations and resonance, which are significant factors in structural failures. However, it can also play beneficial roles, such as

enhancing mixing or heat transfer.[9] Recent studies, including Ericsson[10] and Adjlout and Dixon,[11] have focused on the dynamics of vortex shedding in various configurations, highlighting the critical parameters affecting unsteady flow patterns. Ericsson[10] provided insights into the high-angle-of-attack unsteadiness in slender projectiles, while Adjlout and Dixon[11] examined vortex shedding in turbine cascades, providing a detailed flow visualization of the location of vortices. Frendi[12] and Crouch *et al.*[13] extended this analysis by employing numerical methods and global stability approaches to further understand the onset and characteristics of unsteady flows in different flow regimes.

Type 2 (Unsteadiness due to changes in flow characteristics): Unsteadiness can also arise when fluid properties, such as phase (like phase change material (PCM) flows), density, viscosity, surface temperature, or velocity, undergo continuous and time-dependent changes.[14] For example, a gradually changing surface temperature can generate variable thermal buoyancy, making the secondary flow time-dependent. Numerous studies have delved into such unsteadiness, particularly where thermal effects are present. Yang *et al.*[15] conducted a numerical analysis of unsteady flow in turbocharger turbines, revealing the impact of pulsating flows on turbine performance. Zhang *et al.*[16] studied the unsteady flow over a triangular-section cylindrical at the Reynolds number of 100, analyzing how cylinder inclination affects flow instability and unsteady patterns using quantitative methods. Sanyal and Dhiman[17] explored the wake interactions for two square cylinders influenced by thermal buoyancy impacts, examining Reynolds numbers from 1 to 40, Richardson numbers from 0 to 1, and a Prandtl number of 50.

Type 3: In cases where the geometry is elastic, time-dependent deformations may occur. Similarly, a rigid body may experience oscillatory motions such as plunging or pitching, leading to unsteady flow characteristics. For instance, a pitching airfoil will encounter varying aerodynamic coefficients during its descent and ascent. Frendi[12] provided a detailed investigation into unsteadiness caused by geometric oscillation at different Reynolds numbers, highlighting the influence of oscillation frequency. Studies like Karn *et al.*[18] also focused on geometric oscillations, particularly analyzing their effect on cavitation and unsteady wake formation.

Hwang and Kang[19] numerically analyzed unsteady flow characteristics in an axial compressor, identifying two types of unsteadiness, including stall onset, using a three-dimensional finite-volume solver. In another study, Zhang *et al.*[20] examined flow stability around two circular cylinders arranged in a staggered formation, noting significant perturbation growth in the far-wake region due to the close proximity of cylinders. Similar studies[21,22] have also been performed on elliptical cylinders with varying aspect ratios.

The effects of natural and mixed convection within enclosures containing Newtonian fluids have also been widely studied. These investigations include enclosures with different shapes,[23] inclinations,[24] and boundary conditions.[25–27] Research has explored various cylinder configurations, such as cylinders inside rectangular[28] or concentric enclosures[29] with variable aspect ratios and eccentricities. Jami *et al.*[30] used the lattice Boltzmann method to examine natural convection within a square enclosure, highlighting the cylinder's position as a crucial factor influencing heat transfer and flow patterns. Arif and Hasan[31] explored the performance of different characteristic numerical boundary conditions in mixed convective flow simulations involving a heated square cylinder under a non-Boussinesq approach. This study highlights the importance of properly choosing boundary conditions for achieving accurate results in numerical simulations of mixed convective flows. Öztop *et al.*[32] focused on partially open enclosures, analyzing the impact of geometric parameters on phase change material melting during natural convection. Mixed convection arises when a rotating cylinder is introduced, where forced and buoyancy-driven convection interplay, as observed by Ghaddar and Thiele,[33] who found heat transfer behavior to depend significantly on rotational speed and Rayleigh number. Costa and Raimundo[34] and Liao and Lin[35] extended this understanding by examining the influence of cylinder size, speed, and enclosure geometry on thermal performance.

One phenomenon that can influence an unsteady flow field is the secondary flow induced by thermal buoyancy.[36] When a flow field experiences free convection heat transfer, local variations in flow density can generate a secondary flow, altering the overall flow characteristics.[37] For instance, if thermal buoyancy aligns with the direction of the free stream, it may suppress vortex shedding.[3,4,38] Arif and Hasan[39] conducted a numerical investigation into vortex shedding suppression in mixed convection past a square cylinder subjected to large-scale heating. Using a non-Boussinesq model, they identified a buoyancy parameter that governs the suppression mechanism and highlighted the role of buoyancy and variations in transport properties in controlling vortex shedding. Al-Sumaily *et al.*[40] performed a computational investigation to analyze how thermal buoyancy affects the flow pattern and thermal performance of circular cylinders in a laminar flow regime, covering Reynolds numbers between 20 and 150 and Richardson numbers ranging from 0 to 5, with a constant Prandtl number of 7.1. Their findings demonstrated that as the cylinder's temperature increased, the recirculating flow near the wake dissipated, leading to flow separation only at the rear stagnation point. Furthermore, Ding *et al.*[41] examined vortex-induced vibration in three cylinders arranged in an equilateral triangle under opposing thermal buoyancy using numerical methods. They observed that higher Richardson numbers reduced heat transfer on the up-flow surface of the cylinder while enhancing heat dissipation near the rear stagnation point. Salimipour[3] conducted numerical simulations to investigate the effects of surface temperature variations on flow dynamics and transfer of heat around the horizontal cylinders, accounting for buoyancy forces in 2D, and laminar vertical flows. The study analyzed Grashof number ranging from 0 to 120,000 with fixed Reynolds and Prandtl numbers of 200 and 0.7, respectively. Findings indicated that for the fully isothermal surfaces, the specific Grashof number causes cessation of vortex shedding above the cylinder. In another study, Salimipour[4] examined the influence of mixed convection on thermal and flow characteristics of rotating circular cylinders, with a Prandtl number of 0.7 and Reynolds number of 200, across Grashof numbers ranging from 0 to 120,000 and rotation rates between −4.5 and 4.5. It was observed that clockwise rotation resulted in lower oscillation amplitudes in flow behavior compared to counterclockwise rotation.

Further research has also examined mixed convective heat transfer scenarios involving various geometries and boundary conditions. Basak *et al.*[42] studied mixed convection of air in a square cavity and observed that maximum heat transfer occurred at the edges of the bottom wall rather than at its center. Arif and Hasan[43] examined the impact of both high heating levels and cylinder inclination on mixed convective flows around a square cylinder using a non-Oberbeck–Boussinesq model. Their numerical study revealed that increasing

either the heating level or the inclination angle results in higher drag coefficients while also affecting heat transfer characteristics differently in steady and unsteady regimes. Biswas and Sarkar[44] reported that the critical Richardson number increases with Reynolds number for flow around circular cylinders, highlighting the interplay between buoyancy forces and flow dynamics. The wake characteristics of bluff bodies are further modified when placed in confined domains.[45] Comprehensive investigations have detailed how buoyancy-driven transport affects free-stream flows around different objects under varying Reynolds and Prandtl numbers.[38–40]

Recent studies have continued to explore the complex dynamics of flow around bluff bodies involving vortex shedding, buoyancy effects, and the impact of varying Prandtl numbers. These works highlight the role of thermal gradients and flow unsteadiness in shaping vortex dynamics. Kumar and Dhiman[46] examined how aiding buoyancy and channel confinement can affect heat transfer around a square cylinder, particularly at higher Prandtl numbers. Yu *et al.*[47] explored the impact of thermal buoyancy on flow patterns and heat transfer around porous cylinders, noting that asymmetry in flow occurs after specific ranges of Darcy and Richardson numbers. Garg *et al.*[48] conducted a numerical investigation on mixed convective flow past an elliptical cylinder, examining the effects of varying free-stream orientations and Richardson numbers on aerodynamic parameters. They found that heat transfer generally increased with Richardson number, except for specific orientations, providing insights for compact heat exchanger design. Arif and Hasan[49] investigated thermal buoyancy effects on mixed convection around an inclined square cylinder, identifying a critical Richardson number (Ric = 0.78) that suppressed vortex shedding. Similarly, Ali *et al.*[50] explored the combined influence of Prandtl number, Richardson number, and flow orientation on flow past a heated square cylinder. Their findings showed that higher Richardson numbers led to steady flow at lower Prandtl values, while the flow remained unsteady at 90° inclination. They also observed that the Strouhal number increased with Richardson number but decreased with Prandtl number, highlighting the complex interaction between buoyancy forces and thermal gradients in determining flow behavior.

Despite the numerous recent investigations into flow unsteadiness induced by thermal effects, there remains a gap in understanding the interplay between thermal buoyancy and intrinsic vortex dynamics under varying Prandtl numbers. Moreover, by reviewing and summarizing the results of past research, it can be seen that none of them have studied the effect of continuous changes in flow parameters. In addition, the unsteadiness resulting from the interaction of free stream and thermal buoyancy is not seen in the aforementioned studies. The present study aims to address this by systematically exploring flows with two types of unsteadiness: those arising from the intrinsic nature of the flow (type 1) and those due to changing flow characteristics (type 2). This study examines the laminar flows around a horizontal square cylinder at Reynolds number of 100, where vortex shedding (type 1) naturally occurs. To introduce type 2 unsteadiness, variable thermal buoyancy is applied through changes in surface temperature, leading to a flow with a varying Richardson number ($\mathrm{Ri} = {}^{\mathrm{Gr}}/_{\mathrm{Re}^2}$). A sinusoidal function with different frequencies is used to produce the Richardson numbers. Additionally, the study evaluates the opposing effects of momentum and thermal diffusion by simulating the flow at three different Prandtl numbers: 0.2, 0.7, and 2.5. Figure 1 illustrates the setup of the square cylinder subjected to a vertical free stream.

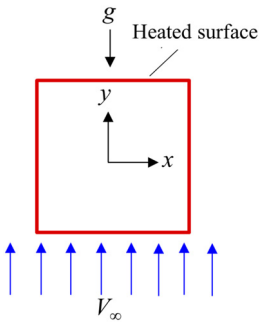

FIG. 1. Configuration of a square cylinder imposed to a vertical free stream.

II. NUMERICAL SOLUTION OF GOVERNING EQUATIONS

In this research, the unsteady and two-dimensional forms of the conservation equations for mass, momentum, and energy are utilized to model heat transfer and fluid flow around a square cylinder. The Boussinesq approximation is applied to account for buoyancy effects, while the energy equation excludes the term associated with viscous dissipation. The governing equations are used in their non-dimensional forms, as described in the referenced literature,[51] and are expressed as follows:

Continuity equation,

$$\frac{\partial u}{\partial x} + \frac{\partial v}{\partial y} = 0. \tag{1}$$

Momentum equations,

$$\frac{\partial(\rho u)}{\partial \tau} + \frac{\partial J_{u-y}}{\partial y} + \frac{\partial J_{u-x}}{\partial x} = -\frac{\partial P}{\partial x}, \tag{2}$$

$$\frac{\partial(\rho v)}{\partial \tau} + \frac{\partial J_{v-y}}{\partial y} + \frac{\partial J_{v-x}}{\partial x} = -\frac{\partial P}{\partial y} + \frac{\mathrm{Gr}}{\mathrm{Re}^2}\Theta. \tag{3}$$

Energy equation,

$$\frac{\partial(\rho\Theta)}{\partial \tau} + \frac{\partial J_{\Theta-y}}{\partial y} + \frac{\partial J_{\Theta-x}}{\partial x} = 0. \tag{4}$$

Here, ρ denotes the density, P represents the pressure, and Θ is the dimensionless temperature. J_{u-y}, J_{u-x}, J_{v-y}, J_{v-x}, $J_{\Theta-y}$, and $J_{\Theta-x}$ include convection and diffusion terms of the momentum and energy equations, defined as follows:

$$\begin{aligned} J_{u-x} &= \rho uu - \frac{1}{\mathrm{Re}}\frac{\partial u}{\partial x} \quad J_{u-y} = \rho uv - \frac{1}{\mathrm{Re}}\frac{\partial u}{\partial y} \\ J_{v-x} &= \rho uv - \frac{1}{\mathrm{Re}}\frac{\partial v}{\partial x} \quad J_{v-y} = \rho vv - \frac{1}{\mathrm{Re}}\frac{\partial v}{\partial y} \\ J_{\Theta-x} &= \rho u\Theta - \frac{1}{\mathrm{Re\,Pr}}\frac{\partial \Theta}{\partial x} \quad J_{\Theta-y} = \rho v\Theta - \frac{1}{\mathrm{Re\,Pr}}\frac{\partial \Theta}{\partial y}. \end{aligned} \tag{5}$$

The Prandtl, Reynolds, and Grashof numbers are defined as follows:[52]

$$\mathrm{Pr} = \frac{\mu C_p}{k}, \quad \mathrm{Re} = \frac{\rho V_\infty a}{\mu}, \quad \mathrm{Gr} = \frac{g\beta\Delta T a^3}{\nu^2}, \tag{6}$$

where the characteristic length is scaled by the cylinder length (a), velocities by the velocity of the free stream (V_∞), time (τ) by a/V_∞, pressure (P) by $\rho {V_\infty}^2$, and the temperature (Θ) is normalized by $(T - T_\infty)/(T_s - T_\infty)$. T_s determines the cylinder's surface temperature.

A custom FORTRAN program was developed to discretize these equations using a finite-volume, cell-centered approach. The pressure–velocity coupling is handled using the RK-SIMPLER scheme, as described in ref. 51. This method solves the momentum and energy equations explicitly, while the pressure equation is derived implicitly from the continuity equation. This method involves solving only one nonlinear equation iteratively for the pressure field, eliminating the need for corrections in the velocity or pressure fields, thus obviating the requirement to solve an approximate pressure correction equation. The Runge–Kutta algorithm is employed to solve the explicit equations for momentum and energy, whereas the Gauss–Seidel method is used to solve the implicit equation for pressure.

In mathematical terms, the balance between convective transport and diffusive dissipation involves two differential operators with different symmetries: the convective derivative is skew-symmetric, while diffusion is described by a symmetric, positive-definite operator. One of the important processes in the finite-volume method is the interpolation of flow quantities on the computational cell faces using several schemes such as upwind, central differencing, MUSCL, and QUICK. The RK-SIMPLER procedure is based on the schemes of upwind family. All upwind schemes have a numerical diffusion due to being one-sided. For this reason, they are not suitable for accurate determination of flow instabilities because they delay the onset of instability (such as vortex shedding onset and transition to 3D flow) by unintentionally removing disturbances. In the present study, due to the importance of vortex shedding ranges, a zero-diffusion scheme based on a second-order central interpolation is used. On the other hand, central schemes are generally unstable and may lead to numerical solution divergence. Verstappen and Veldman[53] solved the instability problem by introducing a method called symmetry-preserving discretization, which preserves the symmetries of the balancing differential operators. In the current article, we develop a powerful zero-diffusion and high-accuracy solver by combining RK-SIMPLER and symmetry-preserving discretization methods. Moreover, the temporal discretization is carried out using the second-order Adams–Bashforth method.

As mentioned above, the Richardson number is made to oscillate using a sinusoidal function defined as follows:

$$\mathrm{Ri}(t) = \mathrm{Ri_m} + \mathrm{Ri_0}\ \sin(k\tau), \tag{7}$$

where $\mathrm{Ri_m}$ and $\mathrm{Ri_0}$ are the mean Richardson number and oscillation amplitude, respectively. k denotes the reduced frequency, which is defined as follows:

$$k = \frac{f\pi a}{V_\infty}. \tag{8}$$

Here, f represents the frequency of oscillation. In this study, the reduced frequency k varies from 0.0001 to 0.1, while a constant value of 0.1 is set for the mean Richardson number and oscillation amplitude.

The outcomes of the numerical simulations include flow contours, vector fields, and streamlines around the cylinder, along with the computed coefficients of drag and lift, which are defined as follows:

$$C_d = \frac{F_d}{\frac{1}{2}\rho V_\infty^2 a}, \tag{9}$$

$$C_l = \frac{F_l}{\frac{1}{2}\rho V_\infty^2 a}, \tag{10}$$

where F_d and F_l represent the drag and lift forces, respectively.

According to the geometry of the problem, using a Cartesian grid could be the best choice. To study the solution independence from the computational grid, three grid sizes of 200×120, 240×140, and 290×170 are tested. Table I compares the average drag coefficients obtained by these grids. The results of grids 2 and 3 are very close together. Therefore, grid 2 with 240×140 cells in vertical and horizontal directions, respectively, is chosen for the current numerical solution. Figure 2 depicts a view of the selected grid. The red line indicates the geometry boundary. The computational domain used in this article is large enough so that the distance of the boundaries of the domain on the left, right, and bottom sides is 10 times the cylinder's length and 40 times on the top side. No-slip boundary conditions were assigned at the cylinder surface, with velocity-inlet and pressure-outlet conditions at the flow boundaries, and symmetry conditions at the lateral boundaries.

III. VALIDATION STUDIES

To achieve the accuracy and reliability of the numerical solver used in this study, the average drag coefficients of a square cylinder at a Reynolds number of 100 were compared against results from previous experimental and numerical studies. The validation was carried out for two scenarios: with and without the influence of thermal buoyancy. The coefficients of mean drag obtained from the current study are presented in Table II, alongside those from other research studies. The discrepancies observed between the results were minimal, with the maximum deviation not exceeding 3%.

As an additional validation measure, the Strouhal numbers corresponding to various Ri (ranging from 0.0 to 0.3) at $\mathrm{Re} = 100$ and $\mathrm{Pr} = 0.7$ were compared with the numerical results provided by Kakade *et al.*[57] Same conditions have been used for the simulation. As illustrated in Fig. 3, a good correspondence between the results is observed.

IV. RESULTS AND ANALYSIS

A. Flow-field analysis for type 1 unsteadiness

The initial instability in the flow past a square cylinder under no-buoyancy conditions emerges at a critical Reynolds number ($\mathrm{Re_{cr}}$) of approximately 45, as noted in prior studies.[58,59] However, the presence

TABLE I. Calculations for the average drag coefficient at Prandtl, Reynolds, and Richardson numbers 0.7, 100, and 0.1, respectively.

	Grid 1 200×120 cells	Grid 2 240×140 cells	Grid 3 290×170 cells
$\bar{C}_d$	1.405	1.476	1.476

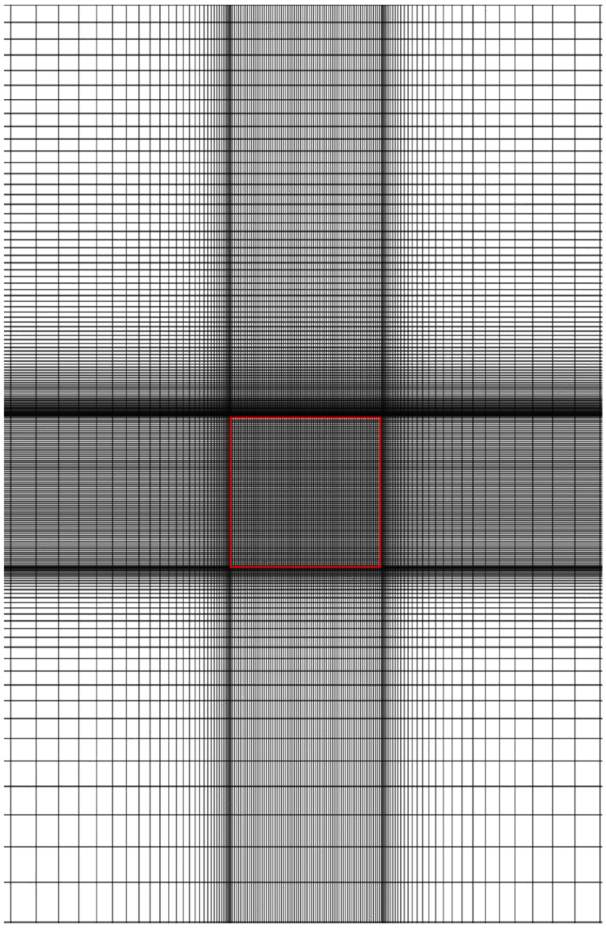

FIG. 2. A view of Cartesian mesh, red line: geometry boundary.

of thermal buoyancy modifies this critical Reynolds number. Specifically, when thermal buoyancy aligns with the direction of the free stream, it enhances the stability of the flow. Consequently, at a fixed Reynolds number, a specific critical Richardson number can be identified where vortex shedding is suppressed, resulting in a steady flow. For instance, at Re = 100 and Pr = 0.7, the critical Richardson number is determined to be 0.125, as illustrated in Fig. 3. The temporal variation of the lift coefficient serves as a method to detect the onset of

TABLE II. Mean drag coefficients comparison of a square cylinder.

Studies (at Pr = 0.7, and Re = 100)			
Ri =	0.0	0.1	0.15
Sohankar *et al.*[54]	1.477	...	...
Darekar and Sherwin (3D)[55]	1.486	...	...
Sahu *et al.*[56]	1.488	...	...
Arif and Hasan[39]	1.510	1.55	1.58
Present	1.486	1.51	1.53

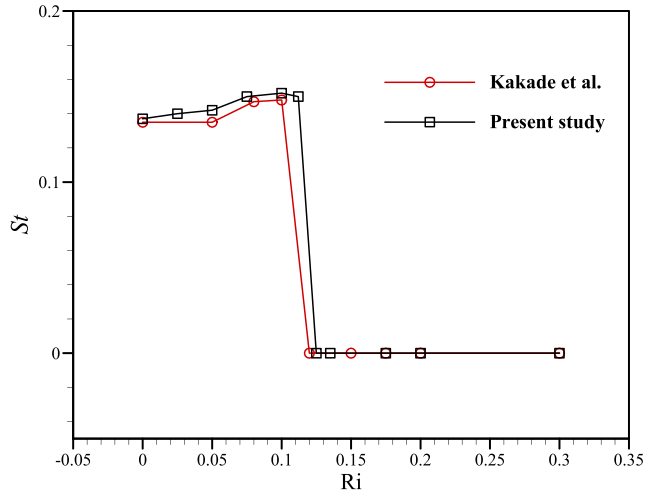

FIG. 3. Comparison between the current Strouhal numbers and the numerical results obtained by Kakade *et al.*[57]

primary instability. Figure 4 illustrates the temporal changes in the lift coefficient at Re = 100 and Pr = 0.7, and various Richardson numbers. The minor disturbances observed within the time interval $20 < \tau < 40$ are attributed to insufficient numerical diffusion in the solver, though these disturbances dissipate over time. As the thermal buoyancy increases, the amplitude of the lift coefficient's oscillations decreases. It is evident that at Ri = 0.125, the oscillations in the lift coefficient are completely suppressed.

This section analyzes type 1 unsteadiness by discretely solving the flow parameters for each Richardson number. The continuous variation of the Richardson number, governed by sine Eq. (7), will be explored in the subsequent section. In this study, Prandtl numbers of 0.2, 0.7, and 2.5 are examined. Figure 5 presents the changes in average drag coefficients across Richardson numbers ranging from 0.0 to 0.2 for these Prandtl numbers. As the Richardson number increases, the drag coefficient rises due to heightened shear stress. At the critical point (Ri = 0.125), a sudden drop in the drag coefficient occurs, coinciding with the elimination of vortex shedding. This reduction becomes more pronounced with higher Prandtl numbers. In fact, removing vortex shedding increases the stability of the flow, which reduces the drag coefficient. But then, the increase in the secondary flow velocity due to increase in the Richardson number increases the drag coefficient. Additionally, an increase in the Prandtl number leads to a decrease in the average drag coefficient for each Richardson number, which can be attributed to enhanced momentum diffusion and, consequently, a reduction in frictional drag. Figure 6 compares the contours and streamlines of non-dimensional temperature at Re = 100 and Pr = 0.7 for Richardson numbers of 0.12 and 0.125. At Ri = 0.12, type 1 unsteadiness is present, while at Ri = 0.125, the formation of two symmetric vortices behind the cylinder indicates stabilization of the flow.

B. Flow-field analysis for type 2 unsteadiness

In the previous subsection, it was demonstrated that when the Richardson number falls below the critical threshold (Ri_{cr}), the flow

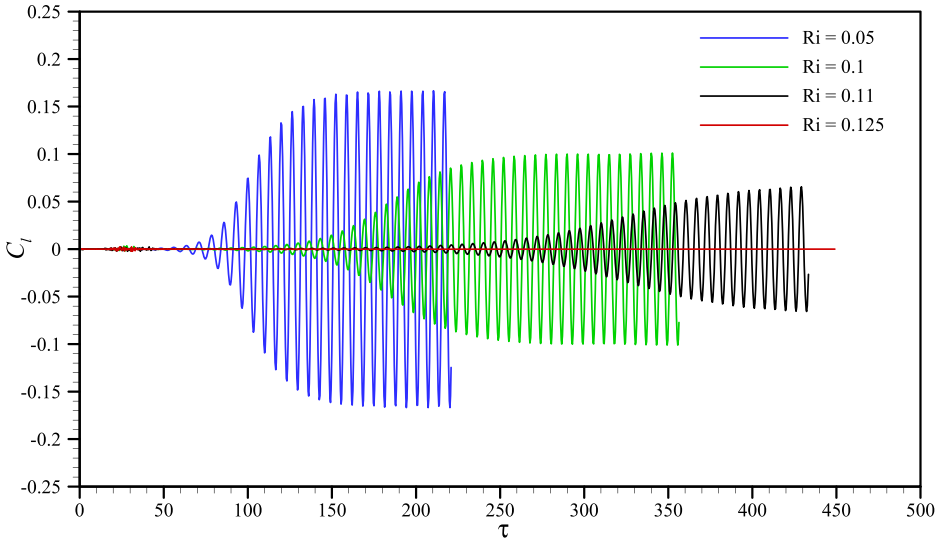

FIG. 4. Variation of cylinder's lift coefficients over time at Reynolds and Prandtl numbers of 100 and 0.7, respectively, for different Richardson numbers.

included type 1 unsteadiness, while for higher Richardson numbers, a steady flow was established. By considering a sinusoidal equation for the Richardson number, type 2 unsteadiness can be formed in the flow field. To prevent the influence of type 1 unsteadiness (vortex shedding), the range of Richardson numbers from 0.15 to 0.35 is investigated. In this range, there is no vortex shedding. According to Eq. (7), for $\mathrm{Ri}_m = 0.25$ and $\mathrm{Ri}_0 = 0.1$, the Richardson number will change between 0.15 and 0.35. For this purpose, by replacing Eq. (7) in the present solver, it is possible to examine the drag coefficient changes at different reduced frequencies. Figure 7 illustrates how the drag coefficient varies in response to continuous changes in the Richardson number for $k = 0.01$, 0.1, and 0.2, alongside the separate solutions representing type 1 unsteadiness at $\mathrm{Re} = 100$ and $\mathrm{Pr} = 0.7$. It can be seen that a hysteresis loop is formed for each reduced frequency. At $k = 0.01$, the drag coefficients in the increasing and decreasing paths

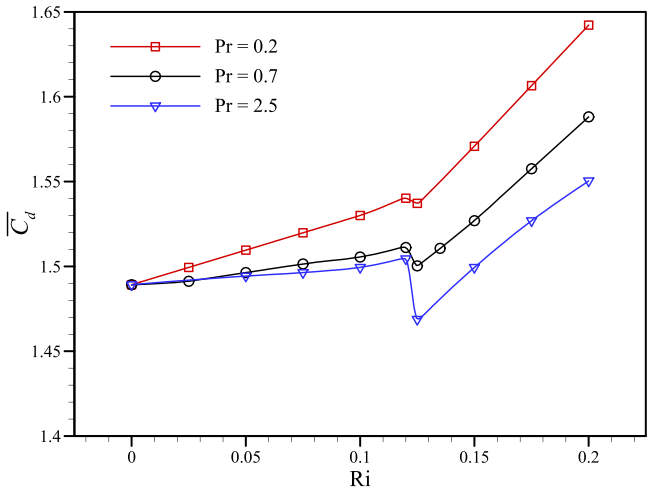

FIG. 5. Illustration of mean drag coefficients as the Richardson number varies for three different Prandtl numbers, with a Reynolds number of 100.

of the Richardson number almost match the type 1 drag coefficients. Therefore, there is no unsteadiness. However, as the reduced frequency (k) increases, the variation rate of Richardson number is intensified and, consequently, the type 2 unsteadiness of the flow increases. For example, at $k = 0.2$ and $\mathrm{Ri} = 0.25$, the difference in drag coefficient in the increasing and decreasing Ri paths is 3.5%.

C. Combination of both unsteadiness effects

If a range of Richardson numbers produced by sinusoidal Eq. (8) is less than the critical Richardson number, the flow will include vortex shedding. In this situation, a combination of type 1 and type 2 unsteadiness occurs. The analysis of such a flow can have interesting physical implications. By choosing $\mathrm{Ri}_m = \mathrm{Ri}_0 = 0.1$, a range of Richardson numbers between 0 and 0.2 is produced, which includes vortex shedding. Figure 8 depicts the variations of the drag coefficients with respect to continuous changes of the Richardson number for $k = 0.001$ and 0.1 along with the separate solutions representing type 1 unsteadiness at $\mathrm{Re} = 100$ and $\mathrm{Pr} = 0.7$. The red area at $k = 0.001$ is formed due to compression of the drag oscillation resulting from vortex shedding. The magnified area shows the oscillation better. The increasing Ri path at $k = 0.1$ also has oscillation resulting from vortex shedding, but because it requires much less time to form a hysteresis loop compared to $k = 0.001$, the oscillations have much less compression. At $k = 0.001$, the increasing Ri path over separate solution points almost coincides, except in the vicinity of the critical Richardson number, where a sudden decrease in drag coefficient did not occur. In fact, type 2 unsteadiness does not occur in the increasing Ri path. In the decreasing Ri path and in the range of Richardson numbers between 0.05 and 0.15, a significant decrease in drag coefficient is observed, so at $\mathrm{Ri} = 0.065$, the difference in drag coefficient in the increasing and decreasing Ri paths is 6%. At $k = 0.1$, completely different drag coefficients than the separate solutions are obtained due to the strengthening effects of the unsteadiness. For example, at $\mathrm{Ri} = 0.0$, the difference in drag coefficient in the increasing Ri path and separate solution is about 5.5%. In addition, by comparing Figs. 7 and 8, it is found that the directions of closed paths are opposite in these two figures. Figure 7

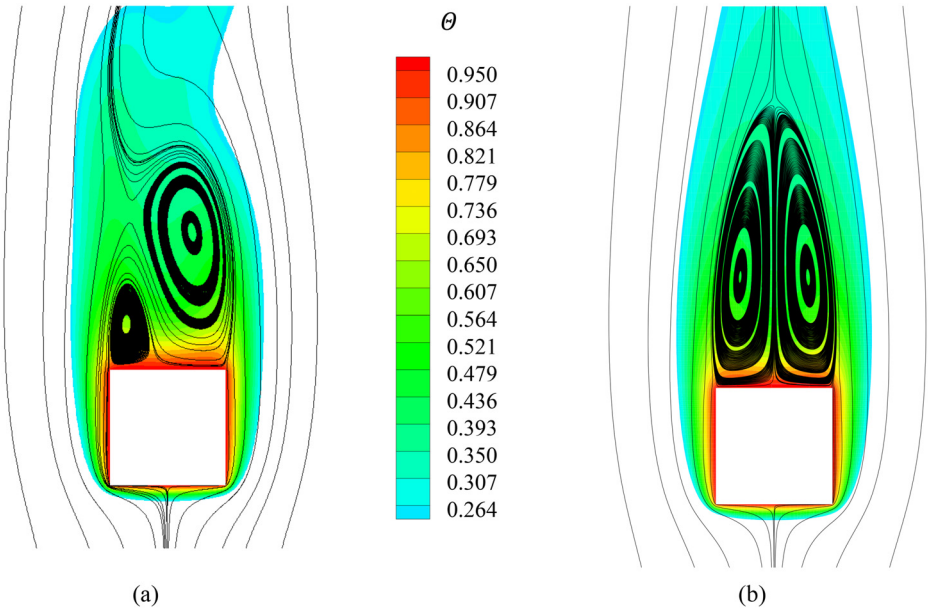

FIG. 6. Temperature contours and streamlines at Reynolds and Prandtl numbers of 100 and 0.7, respectively, at an arbitrary time: (a) Ri = 0.12 (instantaneous streamlines) and (b) Ri = 0.125.

includes larger Richardson numbers that do not include vortex shedding. Therefore, the secondary flow in the decreasing Ri path has more opportunity to stabilize, which leads to an increase in the drag coefficient and, as a result, the production of a counterclockwise loop. However, Fig. 8 includes smaller Richardson numbers that include vortex shedding. In the decreasing Ri path, due to elimination of vortex shedding, the drag coefficient is reduced and, as a result, a clockwise loop is created.

Figure 9 shows the flow patterns around the cylinder for varying Richardson numbers at k = 0.001, Re = 100, and Pr = 0.7. The upper shapes are for the increasing Ri path and the lower shapes are for the decreasing Ri path. As expected, for Ri ≤ 0.1, vortex shedding is observed with the explanation that with increasing Richardson number, the oscillation amplitude of the flow field decreases. For Ri ≥ 0.15 in the increasing Ri path, a steady flow consisting of two symmetrical vortices is formed. However, at Ri = 0.2, a smaller vortical area is observed compared to Ri = 0.15. In the decreasing Ri path for Ri ≥ 0.07, the steady flow is still maintained and as expected, as the

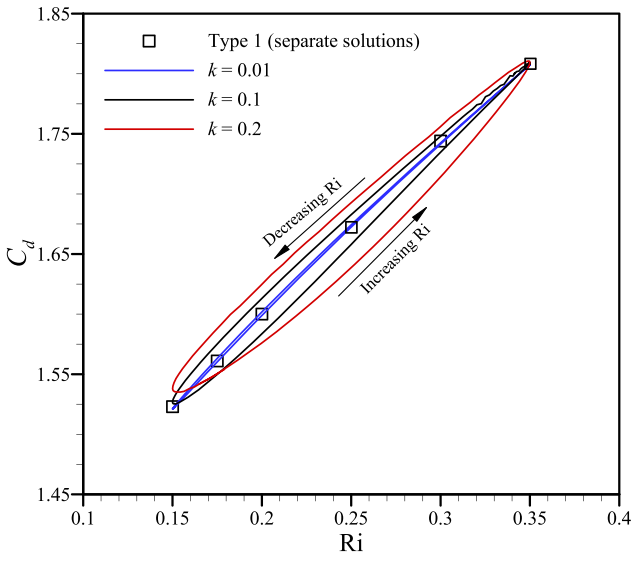

FIG. 7. Hysteresis loops of drag coefficient for $k = 0.01$, 0.1, and 0.2 along with separate solutions representing type 1 unsteadiness at Re = 100 and Pr = 0.7.

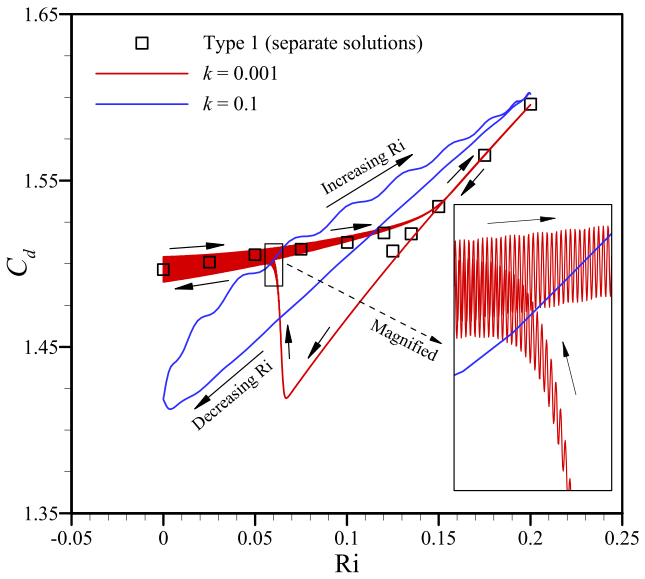

FIG. 8. Hysteresis loops of drag coefficient vs the sinusoidal Richardson number for $k = 0.001$ and 0.1 along with separate solutions representing type 1 unsteadiness at Pr = 0.7 and Re = 100.

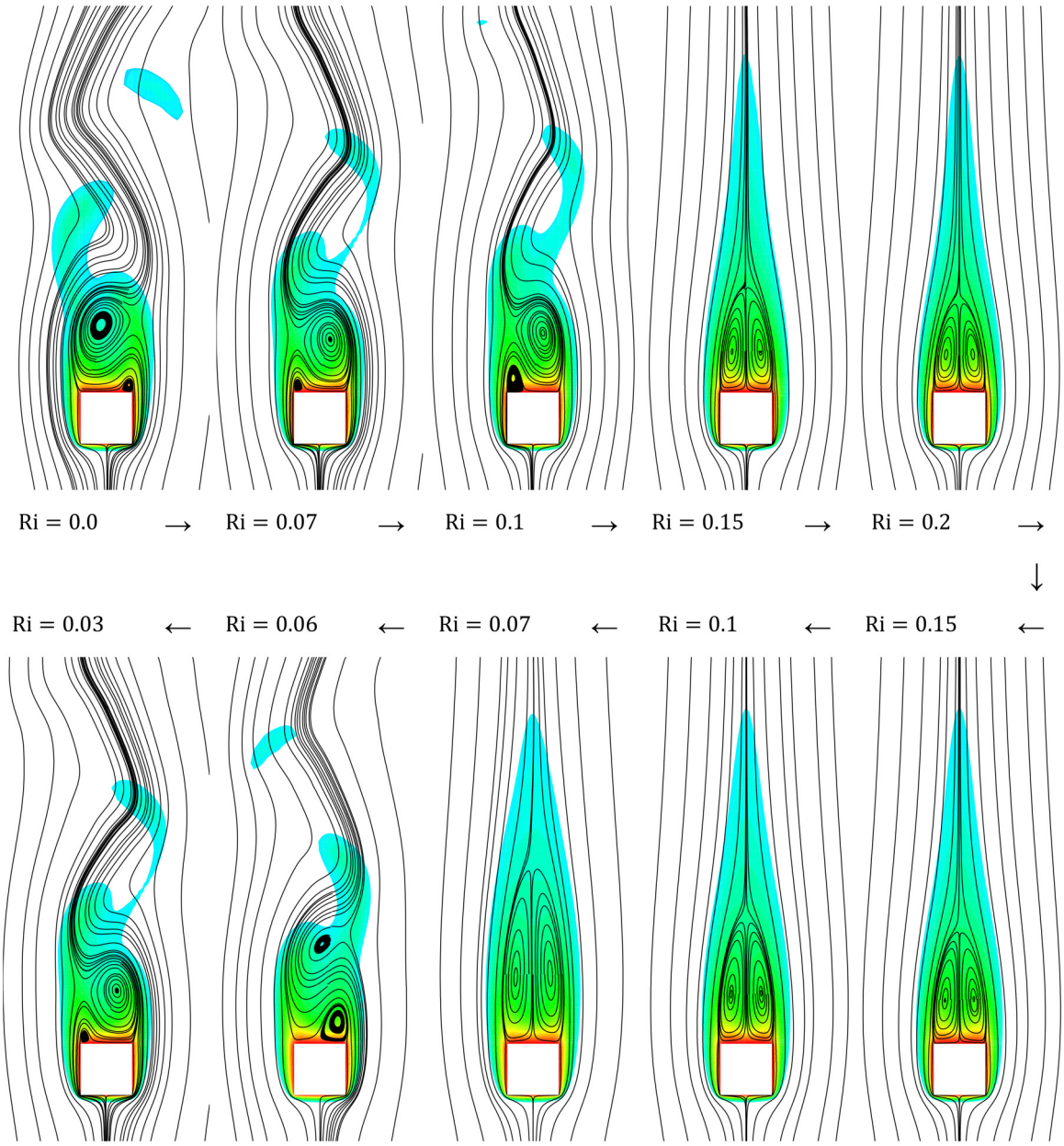

FIG. 9. Flow patterns and contours of temperature at Re = 100, and Pr = 0.7, and $k = 0.001$. The direction of arrows shows the hysteresis loop of Richardson numbers.

Richardson number decreases, the vortices become larger. For $Ri \leq 0.06$, type 1 unsteadiness prevails and causes vortex shedding.

Figure 10 depicts the variations of the drag coefficients with respect to continuous changes of the Richardson number for four different reduced frequencies at Re = 100 and Pr = 0.7. In order to better see the hysteresis loops, the oscillating regions of the drag coefficients are time averaged. As the reduced frequency decreases, the drag coefficient values become closer to the separated solutions. At $k = 0.0001$, except near the critical point ($Ri = 0.125$), there is very good agreement with the separated solution points. In fact, at this frequency, the flow finds enough opportunity to form under the applied thermal buoyancy. The lowest drag coefficient in the examined cases occurs at $k = 0.01$, which is at $Ri = 0.03$ with a value of 1.375. The difference in drag coefficient in the increasing and decreasing Ri paths at this point is 8.5%. Furthermore, at $k = 0.1$, the curve trend is different compared to that at the other reduced frequencies. At $k = 0.1$, the flow has not enough time to change the structure. Therefore, the effects of thermal buoyancy at different Richardson numbers are integrated into each other.

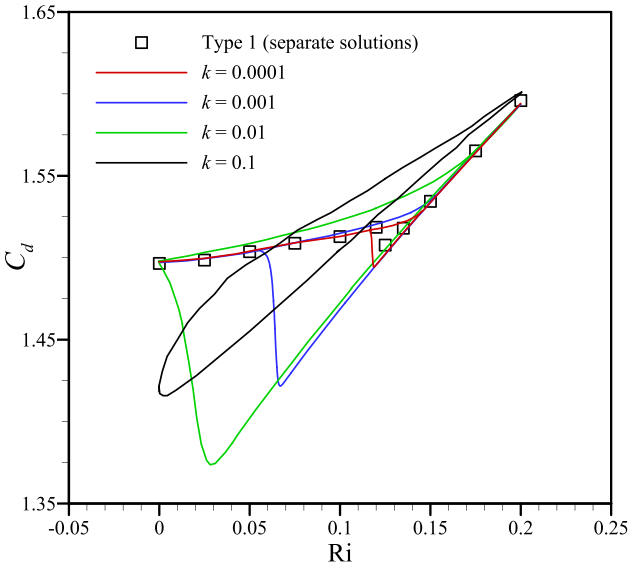

FIG. 10. Hysteresis loops of time-averaged drag coefficient with respect to continuous Richardson numbers for several reduced frequencies at Re = 100 and Pr = 0.7.

V. CONCLUSIONS

This paper numerically studied the unsteady flow around a horizontal square cylinder along with the thermal buoyancy effects for Re = 100, $0.0 \leq Ri \leq 0.35$, and Pr = 0.2, 0.7, and 2.5. The effects of two unsteadiness types (type1: vortex shedding, type 2: variable Richardson number) on the flow patterns and characteristics were investigated in separate situations and combined form. A finite-volume pressure–velocity coupling scheme was used to numerically solve the flow field and temperature field. To avoid numerical errors due to undesirable damping effects, a second-order, central symmetry-preserving method was used, which preserved the symmetries of the balancing differential operators. The results were categorized into three sections as follows: flow-field analysis for type 1 unsteadiness, flow-field analysis for type 2 unsteadiness, and combination of both unsteadiness effects. In type 1 unsteadiness, a critical Richardson number was found to eliminate the vortex shedding and formed a steady flow. For example, the critical Richardson number at Re = 100 and Pr = 0.7 was 0.125. In type 2 unsteadiness, a sinusoidal equation was used to generate variable Richardson number. A hysteresis loop was formed for each reduced frequency. As the reduced frequency increased, the variation rate of the Richardson number was amplified and, consequently, type 2 unsteadiness of the flow increased. In the third study, by combining the two unsteadiness effects, it was observed that the overall unsteadiness effect was increased. At $k = 0.001$, for $Ri \geq 0.15$ in the increasing Ri path, a steady flow was formed. In the decreasing Ri path for $Ri \geq 0.065$, the steady flow is still maintained and, as expected, as the Richardson number decreased, the vortices became larger. For $Ri \leq 0.065$, type 1 unsteadiness prevails and causes vortex shedding. Moreover, except in the vicinity of the critical point, there was a strong agreement with the distinct solution points. In addition, at $k = 0.1$, the curve trend was different compared to that at other reduced frequencies because the flow had not enough time to change its structure. Therefore, the effects of thermal buoyancy under different Richardson numbers were integrated into each other.

ACKNOWLEDGMENTS

This research of Mikhail Sheremet and Mohammad Ghalambaz was supported by the Tomsk State University Development Programme (Priority-2030).

AUTHOR DECLARATIONS

Conflict of Interest

The authors have no conflicts to disclose.

Author Contributions

Shima Yazdani: Investigation (equal); Validation (equal); Writing – original draft (equal); Writing – review & editing (equal). **Erfan Salimipour:** Conceptualization (equal); Investigation (equal); Methodology (equal); Validation (equal); Visualization (equal); Writing – original draft (equal); Writing – review & editing (equal). **Mikhail A. Sheremet:** Methodology (equal); Supervision (equal); Visualization (equal); Writing – review & editing (equal). **Mohammad Ghalambaz:** Formal analysis (equal); Methodology (equal); Supervision (equal); Visualization (equal); Writing – review & editing (equal).

DATA AVAILABILITY

The data that support the findings of this study are available from the corresponding author upon reasonable request.

REFERENCES

[1]N. Michaux-Leblond and M. Bélorgey, "Near-wake behavior of a heated circular cylinder: Viscosity-buoyancy duality," Exp. Therm. Fluid Sci. **15**(2), 91–100 (1997).
[2]S. Mittal and B. Kumar, "Flow past a rotating cylinder," J. Fluid Mech. **476**, 303–334 (2003).
[3]E. Salimipour, "A numerical study on the fluid flow and heat transfer from a horizontal circular cylinder under mixed convection," Int. J. Heat Mass Transfer **131**, 365–374 (2019).
[4]E. Salimipour, "Thermal buoyancy effects on the flow field and heat transfer of a rotating cylinder: A numerical study," Int. J. Therm. Sci. **155**, 106453 (2020).
[5]E. Salimipour and H. Dayani, "Investigating the characteristics of flow past an elliptic moving belt," Ocean Eng. **267**, 113296 (2023).
[6]E. Salimipour and S. Yazdani, "Study on the fluid flow and heat transfer characteristics of a horizontal elliptical cylinder under thermal buoyancy effect," Int. J. Heat Mass Transfer **192**, 122948 (2022).
[7]E. Salimipour, S. Yazdani, and M. Ghalambaz, "Flow field analysis of an elliptical moving belt in transitional flow regime," Eur. Phys. J. Plus **136**(7), 783 (2021).
[8]N. K. Chaitanya, S. Khambra, and D. Chatterjee, "Mixed convective transport around tandem circular cylinders in an unconfined medium," Nucl. Eng. Des. **419**, 112969 (2024).
[9]K.-S. Chang and J.-Y. Sa, "The effect of buoyancy on vortex shedding in the near wake of a circular cylinder," J. Fluid Mech. **220**, 253–266 (1990).
[10]L. E. Ericsson, "Flow unsteadiness considerations in high-alpha testing," J. Aircraft **25**(11), 1033–1037 (1988).
[11]L. Adjlout and S. L. Dixon, "Endwall losses and flow unsteadiness in a turbine blade cascade," J. Turbomach. **114**(1), 191–197 (1992).
[12]A. Frendi, "On flow unsteadiness induced by structural vibration," J. Sound Vib. **269**(1–2), 327–343 (2004).

[13]J. D. Crouch, A. Garbaruk, and D. Magidov, "Predicting the onset of flow unsteadiness based on global instability," J. Comput. Phys. **224**(2), 924–940 (2007).
[14]M. Ghalambaz, M. Sheremet, K. Shank, S. Tiari, and M. Fteiti, "Improving phase change heat transfer in an enclosure partially filled by uniform and anisotropic metal foam layers," Int. J. Heat Mass Transfer **228**, 125678 (2024).
[15]M. Yang, K. Deng, R. Martines-Botas, and W. Zhuge, "An investigation on unsteadiness of a mixed-flow turbine under pulsating conditions," Energy Convers. Manage. **110**, 51–58 (2016).
[16]W. Zhang, H. Yang, H.-S. Dou, and Z. Zhu, "Flow unsteadiness and stability characteristics of low-re flow past an inclined triangular cylinder," J. Fluids Eng. **139**(12), 121203 (2017).
[17]A. Sanyal and A. Dhiman, "Wake interactions in a fluid flow past a pair of side-by-side square cylinders in presence of mixed convection," Phys. Fluids **29**(10), 103602 (2017).
[18]A. Karn, R. E. A. Arndt, and J. Hong, "Dependence of supercavity closure upon flow unsteadiness," Exp. Therm. Fluid Sci. **68**, 493–498 (2015).
[19]Y. Hwang and S.-H. Kang, "Numerical study on near-stall flow unsteadiness in an axial compressor with casing treatment," J. Mech. Sci. Technol. **27**(8), 2375–2381 (2013).
[20]W. Zhang, X. Li, and Z. Zhu, "Quantification of wake unsteadiness for low-Re flow across two staggered cylinders," Proc. Inst. Mech. Eng., Part C: J. Mech. Eng. Sci. **233**(19–20), 6892–6909 (2019).
[21]W. Zhang and X. Su, "Effect of surface curvature on destabilization and unsteadiness of low-Re flow across two tandem elliptic cylinders," Proc. Inst. Mech. Eng., Part C: J. Mech. Eng. Sci. **235**(22), 6080–6098 (2021).
[22]A. Pradhan, M. R. Arif, M. S. Afzal, and A. H. Gazi, "On the origin of forces in the wake of an elliptical cylinder at low Reynolds number," Environ. Fluid Mech. **22**(6), 1307–1331 (2022).
[23]A. Saha, N. K. Manna, K. Ghosh, and N. Biswas, "Analysis of geometrical shape impact on thermal management of practical fluids using square and circular cavities," Eur. Phys. J. Spec. Top. **231**(13), 2509–2537 (2022).
[24]A. Baïri, E. Zarco-Pernia, and J.-M. G. De María, "A review on natural convection in enclosures for engineering applications. The particular case of the parallelogrammic diode cavity," Appl. Therm. Eng. **63**(1), 304–322 (2014).
[25]T. Pesso and S. Piva, "Laminar natural convection in a square cavity: Low Prandtl numbers and large density differences," Int. J. Heat Mass Transfer **52**(3–4), 1036–1043 (2009).
[26]Q.-H. Deng, "Fluid flow and heat transfer characteristics of natural convection in square cavities due to discrete source–sink pairs," Int. J. Heat Mass Transfer **51**(25–26), 5949–5957 (2008).
[27]N. B. Khedher, M. Sheremet, A. M. Hussin, S. A. M. Mehryan, and M. Ghalambaz, "The effect of hot wall configuration on melting flow of nano-enhanced phase change material inside a tilted square capsule," J. Energy Storage **69**, 107921 (2023).
[28]F. Moukalled and S. Acharya, "Natural convection in the annulus between concentric horizontal circular and square cylinders," J. Thermophys. Heat Transfer **10**(3), 524–531 (1996).
[29]T. Kuehn and R. Goldstein, "An experimental and theoretical study of natural convection in the annulus between horizontal concentric cylinders," J. Fluid Mech. **74**(4), 695–719 (1976).
[30]M. Jami, A. Mezrhab, and H. Naji, "Numerical study of natural convection in a square cavity containing a cylinder using the lattice Boltzmann method," Eng. Computations **25**(5), 480–489 (2008).
[31]M. R. Arif and N. Hasan, "Performance of characteristic numerical boundary conditions for mixed convective flows past a heated square cylinder using a non-Boussinesq approach," Numer. Heat Transfer, Part A: Appl. **76**(4), 254–280 (2019).
[32]H. F. Öztop, H. Coşanay, F. Selimefendigil, and N. Abu-Hamdeh, "Analysis of melting of phase change material block inserted to an open cavity," Int. Commun. Heat Mass Transfer **137**, 106240 (2022).
[33]N. Ghaddar and F. Thiele, "Natural convection over a rotating cylindrical heat source in a rectangular enclosure," Numer. Heat Transfer **26**(6), 701–717 (1994).
[34]V. Costa and A. Raimundo, "Steady mixed convection in a differentially heated square enclosure with an active rotating circular cylinder," Int. J. Heat Mass Transfer **53**(5–6), 1208–1219 (2010).
[35]C.-C. Liao and C.-A. Lin, "Mixed convection of a heated rotating cylinder in a square enclosure," Int. J. Heat Mass Transfer **72**, 9–22 (2014).
[36]M. Ghalambaz, H. Arasteh, R. Mashayekhi, A. Keshmiri, P. Talebizadehsardari, and W. Yaïci, "Investigation of overlapped twisted tapes inserted in a double-pipe heat exchanger using two-phase nanofluid," Nanomaterials **10**(9), 1656 (2020).
[37]M. Ghalambaz, T. Groşan, and I. Pop, "Mixed convection boundary layer flow and heat transfer over a vertical plate embedded in a porous medium filled with a suspension of nano-encapsulated phase change materials," J. Mol. Liq. **293**, 111432 (2019).
[38]E. Salimipour, "Three-dimensionality effects on the flow past a horizontal heated cylinder under mixed convection heat transfer," Phys. Fluids **35**(11), 114109 (2023).
[39]M. R. Arif and N. Hasan, "Vortex shedding suppression in mixed convective flow past a square cylinder subjected to large-scale heating using a non-Boussinesq model," Phys. Fluids **31**(2), 023602 (2019).
[40]G. F. Al-Sumaily, H. A. Dhahad, H. M. Hussen, and M. C. Thompson, "Influence of thermal buoyancy on vortex shedding behind a circular cylinder in parallel flow," Int. J. Therm. Sci. **156**, 106434 (2020).
[41]L. Ding, H. He, and T. Song, "Vortex-induced vibration and heat dissipation of multiple cylinders under opposed thermal buoyancy," Ocean Eng. **270**, 113669 (2023).
[42]T. Basak, S. Roy, P. K. Sharma, and I. Pop, "Analysis of mixed convection flows within a square cavity with uniform and non-uniform heating of bottom wall," Int. J. Therm. Sci. **48**(5), 891–912 (2009).
[43]M. R. Arif and N. Hasan, "Large-scale heating effects on global parameters for flow past a square cylinder at different cylinder inclinations," Int. J. Heat Mass Transfer **161**, 120237 (2020).
[44]G. Biswas and S. Sarkar, "Effect of thermal buoyancy on vortex shedding past a circular cylinder in cross-flow at low Reynolds numbers," Int. J. Heat Mass Transfer **52**(7–8), 1897–1912 (2009).
[45]G. Gandikota, S. Amiroudine, D. Chatterjee, and G. Biswas, "The effect of aiding/opposing buoyancy on two-dimensional laminar flow across a circular cylinder," Numer. Heat Transfer, Part A: Appl. **58**(5), 385–402 (2010).
[46]D. Kumar and A. K. Dhiman, "Effects of aiding buoyancy and channel confinement on the flow and heat transfer of dilatant fluids from a square obstacle," Comput. Therm. Scien. **10**(2), 121 (2018).
[47]S. Yu, T. Tang, J. Li, and P. Yu, "Wake and thermal characteristics for cross-buoyancy mixed convection around and through a porous cylinder," Phys. Fluids **32**(7), 073603 (2020).
[48]A. Garg, M. R. Arif, and N. Hasan, "Impact of free-stream orientation and thermal buoyancy on aerodynamic and heat transfer characteristics in mixed convective flow past an elliptical cylinder," Phys. Fluids **36**(7), 073613 (2024).
[49]M. R. Arif and N. Hasan, "Effect of thermal buoyancy on vortex-shedding and aerodynamic characteristics for fluid flow past an inclined square cylinder," Int. J. Heat Technol. **38**(2), 463 (2020).
[50]R. Ali, M. R. Arif, S. A. Haider, and F. A. Shamim, "Effect of Prandtl number and free-stream orientation on global parameters for flow past a heated square cylinder," Phys. Fluids **36**(3), 033602 (2024).
[51]R. G. Rajagopalan and A. D. Lestari, "RK-SIMPLER: Explicit Time-accurate algorithm for incompressible flows," AIAA J. **54**(2), 616–624 (2016).
[52]A. Arshadi, M. Nili-Ahmadabadi, A. Minaeian, and M. Y. Ha, "Mixed-convection flow and heat transfer in a square enclosure around a rotating hot cylinder immersed in a Phan-Thien–Tanner viscoelastic fluid," Int. J. Heat Mass Transfer **229**, 125710 (2024).
[53]R. W. C. P. Verstappen and A. E. P. Veldman, "Symmetry-preserving discretization of turbulent flow," J. Comput. Phys. **187**(1), 343–368 (2003).
[54]A. Sohankar, C. Norberg, and L. Davidson, "Low-Reynolds-number flow around a square cylinder at incidence: Study of blockage, onset of vortex

shedding and outlet boundary condition," Int. J. Numer. Meth. Fluids **26**(1), 39–56 (1998).
[55]R. M. Darekar and S. J. Sherwin, "Flow past a square-section cylinder with a wavy stagnation face," J. Fluid Mech. **426**, 263–295 (2001).
[56]A. K. Sahu, R. P. Chhabra, and V. Eswaran, "Two-dimensional unsteady laminar flow of a power law fluid across a square cylinder," J. Non-Newtonian Fluid Mech. **160**(2–3), 157–167 (2009).
[57]A. A. Kakade, S. K. Singh, P. K. Panigrahi, and K. Muralidhar, "Schlieren investigation of the square cylinder wake: Joint influence of buoyancy and orientation," Phys. Fluids **22**(5), 054107 (2010).
[58]D. Park and K.-S. Yang, "Flow instabilities in the wake of a rounded square cylinder," J. Fluid Mech. **793**, 915–932 (2016).
[59]D.-H. Yoon, K.-S. Yang, and C.-B. Choi, "Flow past a square cylinder with an angle of incidence," Phys. Fluids **22**(4), 043603 (2010).